Journal of Magnetism and Magnetic Materials 563 (2022) 169858

Contents lists available at ScienceDirect

Journal of Magnetism and Magnetic Materials

journal homepage: www.elsevier.com/locate/jmmm

Voltage-induced terahertz magnon excitation associated with antiferromagnetic domain wall precession

Xu Ge [a], Yangyi Chen [a], Zaidong Li [b], Peng Yan [c,*], Hong-Guang Piao [d], Wei Luo [a], Shiheng Liang [e], Xiaofei Yang [a], Long You [a], Yue Zhang [a,*]

[a] School of Optical and Electronic Information, Huazhong University of Science and Technology, Wuhan 430074, China
[b] School of Science, Tianjin University of Technology, Tianjin 300384, China
[c] School of Electronic Science and Engineering and State Key Laboratory of Electronic Thin Films and Integrated Devices, University of Electronic Science and Technology of China, Chengdu 610054, China
[d] Department of Physics, College of Science, Yanbian University, Yanji 133002, China
[e] Department of Physics, Hubei University, Wuhan 430062, China

ARTICLE INFO

Keywords:
Terahertz magnon
Antiferromagnet
Domain wall precession
Anisotropy energy gradient

ABSTRACT

Exploring a low-power method for exciting terahertz (THz) signals is of great interest in developing devices with ultrafast signal processing. We numerically investigated the THz magnon excitation from a moving antiferromagnetic (AFM) domain wall (DW) driven by a voltage-induced magnetic anisotropy energy gradient (dE_a/dx). This magnon excitation originates from the DW precession induced by dE_a/dx. Unlike the AFM DW precession triggered by DW acceleration as predicted in previous investigation, the dE_a/dx-induced DW precession is possible when the DW acceleration is negligible. When the frequency of DW precession is greater than the frequency gap of spin-wave propagation in the AFM medium, THz magnons are resonantly excited. Because dE_a/dx can be generated under a moderate DC voltage, our work provides a potential approach for developing THz spintronic devices with a low power and dissipation.

1. Introduction

An antiferromagnetic (AFM) medium is a promising candidate for the emission of THz electromagnetic waves, which have extraordinary potential applications in high-speed wireless communication, medical imaging, security, and material characterization [1–5]. In principle, THz spin oscillation in an AFM medium originates from strong exchange coupling between neighboring spins [1,5]. In experiments, AFM THz dynamics is generally excited by a femtosecond pulsed laser [6–9] that requires a high power and gives rise to the side effect of heating. Therefore, exploring the method for exciting AFM THz spin oscillation with a low power consumption is critically important.

Many investigations concentrate on intrinsic AFM dynamics by assuming a spatially uniform spin structure in AFM materials [10–13]. However, in a real AFM medium, there exist textures with complicated spin structures, such as vortices, domain walls (DWs), and skyrmions [14–17]. Usually, a moving DW is a source for exciting spin oscillation (spin wave or magnon). For example, a moving ferromagnetic DW can emit GHz spin wave [18–20]. Nevertheless, the investigation of the THz spin-wave emission (magnon excitation) from a moving AFM DW is still very few due to the lack of an easy driving method in the past. This has changed in the last decade thanks to the research progress in spintronics and multiferroics. A collinear AFM DW can be triggered to move by spin–orbit torque (SOT), electric field, spin wave, or temperature gradient [21–32]. A moving AFM DW behaves like a massive relativistic particle: DW velocity may not exceed the maximum group velocity of an AFM spin wave (c_{max}) [21,33,34]. When the DW velocity approaches c_{max}, DW width significantly shrinks (Lorentz contraction), which is accompanied by the emission of a THz spin wave [21,33]. In addition to the magnon excitation by the relativistic Lorentz contraction of an AFM DW [21], another spin-wave emission was also theoretically predicted by variable AFM DW motion [35,36]. It turns out that a nonzero AFM DW acceleration is necessary for DW precession and spin-wave emission [35].

In this study, based on numerical calculation, we predict the excitation of DW precession and THz magnon from a moving AFM DW under an anisotropy gradient (dE_a/dx). Unlike the previous AFM DW precession coupled with DW acceleration, the dE_a/dx-induced DW precession

* Corresponding authors.
E-mail addresses: yan@uestc.edu.cn (P. Yan), yue-zhang@hust.edu.cn (Y. Zhang).

https://doi.org/10.1016/j.jmmm.2022.169858
Received 28 June 2022; Received in revised form 1 August 2022; Accepted 18 August 2022
Available online 5 September 2022

is possible even when the DW acceleration is negligible. When the frequency of DW precession is greater than the frequency gap for the AFM spin-wave propagation, resonant THz magnons can be excited. In experiments, the dE_a/dx can be generated by the technique as displayed in Fig. 1: A DC voltage applied across the wedge-shaped insulating layer generates dE_a/dx, which triggers the AFM DW to move towards the end with a lower magnetic anisotropy constant [37–40]. This method for manipulating anisotropy was not only put forward in theory [37–40] but also realized in the experiment [41].

2. Model and methods

We considered the dE_a/dx-induced DW motion in a 1-dimensional (1D) AFM chain [dimension: 252 nm (length) × 0.42 nm (width) × 0.42 nm (thickness)] consisted of two sublattices (I and II). The Hamiltonian of the 1D AFM chain is.

$$H = J\sum_i \vec{S}^{(i)}\cdot\vec{S}^{(i+1)} - K_z d^3\sum_i(\vec{S}^{(i)}\cdot\vec{e}_z)^2 - K_x d^3\sum_i\left(\vec{S}^{(i)}\cdot\vec{e}_x\right)^2 \quad (1)$$

Here $\vec{S}^{(i)}$ is the normalized spin at site i. The first term on the right-hand side of Eq. (1) is the exchange energy with an exchange integral J ($J > 0$). The second term represents the easy-axis anisotropy energy along the z-axis direction with an anisotropy constant K_z ($K_z > 0$). We also considered a small anisotropy energy along the x-axis direction with a coefficient K_x ($K_x > 0$) to stabilize a Néel-type AFM DW as the initial state. This biaxial anisotropy widely exists in a magnetic medium due to magnetocrystalline anisotropy, stress anisotropy, or electric-field-induced anisotropy [42,43].

The dynamics of $\vec{S}^{(i)}$ is governed by the Landau-Lifshitz-Gilbert equation:

$$\frac{\partial\vec{S}^{(i)}}{\partial t} = -\gamma\vec{S}^{(i)}\times\vec{H}_{eff}^{(i)} + \alpha\vec{S}^{(i)}\times\frac{\partial\vec{S}^{(i)}}{\partial t} \quad (2)$$

where γ, α, and $\vec{H}_{eff}^{(i)}$ denote the gyromagnetic ratio of an electron, Gilbert damping parameter, and effective field ($\vec{H}_{eff}^{(i)} = -\frac{\partial H}{\mu_0 M_S d^3\partial\vec{S}^{(i)}}$), respectively. Here μ_0 and M_S are the permeability of vacuum and saturation magnetization. For numerical calculations, the AFM chain was divided into meshes labeled i ($i = 1, 2, 3\ldots$) with dimension 0.42 nm × 0.42 nm × 0.42 nm. Eq. (2) was numerically solved using the fourth-order Runge–Kutta method with a time step$\Delta t = 0.1$ ps. We exploited the parameters of NiO with $M_S = 4.25 \times 10^5$ A/m (1.7 μ_B magnetic moment for each Ni ion, two spin-up and two spin-down Ni ions in a mesh); $J = 2.1 \times 10^{-22}$ J [44–47]; $K = K_0 + s(x - 21.84\ \text{nm})$, where $K_0 = 3.8 \times 10^5$ J/m^3 is the anisotropy constant at $x = 21.84$ nm, the initial DW position. s is the anisotropy gradient ranging from − 200 to − 1400 GJ/m^4. $K_x = 5.7 \times 10^4$ J/m^3. $d = 0.42$ nm, the lattice constant of NiO [23,44]. To avoid magnon reflection [48], near the two ends of the chain we employed a damping coefficient with a linear function of x as $\alpha = -0.1428i + 1$ [$i = (x/0.42\ \text{nm}) + 1$] in the region 0 nm $\le x <$ 2.94 nm, and $\alpha = 0.1428i - 84.814$ [$i = (x/0.42\ \text{nm}) + 1$] in the region 249.06 nm $< x \le$ 252 nm.

3. Results and discussion

We defined the Néel vector $\vec{n}(\vec{r},t) = [\vec{M}_I(\vec{r},t) - \vec{M}_{II}(\vec{r},t)]/l(\vec{r},t)$ with $l(\vec{r},t) = \left|\vec{M}_I(\vec{r},t) - \vec{M}_{II}(\vec{r},t)\right| \approx 2M_S$(Fig. 1) and total magnetization $\vec{M} = \left[\vec{M}_I(\vec{r},t) + \vec{M}_{II}(\vec{r},t)\right]$ to quantify the AFM dynamics. We derived the x, y, and z components of the Néel vector (n_x, n_y, and n_z) based on the numerical solution of Eq. (2).

Initially, the DW exhibited a Néel-type structure [Fig. 2(a)]. As shown in Fig. 2(b), under anisotropy gradient $s = -1400$ GJ/m^4, the DW moved towards the right end with a lower anisotropy energy, which was accompanied by the magnon emission towards the DW stern [The movie for this magnon excitation was exhibited in the Supplementary Materials (S1).]. At both $t = 0$ and 400 ps, the DW profile can be well fitted by the Walker function (the solid blue lines):$n_z = \cos[2\arctan(x - X)/\lambda]$. Here X and λ are the central position and the width of the DW. The fitted λ kept almost constant in the initial 100 ps and substantially increased afterwards [Fig. 2(c)]. This is in sharp contrast to that emitted from an AFM DW moving at a high velocity with a significant contraction of DW width [21,34].

Based on the snapshots of n_x at various time for $s = -1400$ GJ/m^4, we found that magnon excitation started at around 100 ps [Fig. 2(d)]. As shown in Fig. 2(e), representative n_x oscillation from a moving AFM DW was exhibited at $x = 22.26$ nm, which is near the left end of the chain. A series of wave packages were seen, which indicates that the magnon frequency varied with DW motion. The inset of Fig. 2(e) shows the period for the n_x oscillation near 500 ps is clearly shorter than that near 150 ps. Furthermore, the magnon spectra were derived by converting the time-domain n_x into a frequency-domain one through 1D fast Fourier transformation (FFT) (sampling between 100 ps ~ 550 ps with an interval of 0.1 ps). The spectra demonstrated a series of peaks from 0.2 THz to 0.35 THz with a gradually increased amplitude. After 550 ps, the DW approached the right end of the chain, leading to the clear depression of the magnon amplitude at a higher frequency.

The increase of magnon frequency may originate from the broadened DW width [Fig. 2(c)], which reduces the DW mass and thus gives rise to

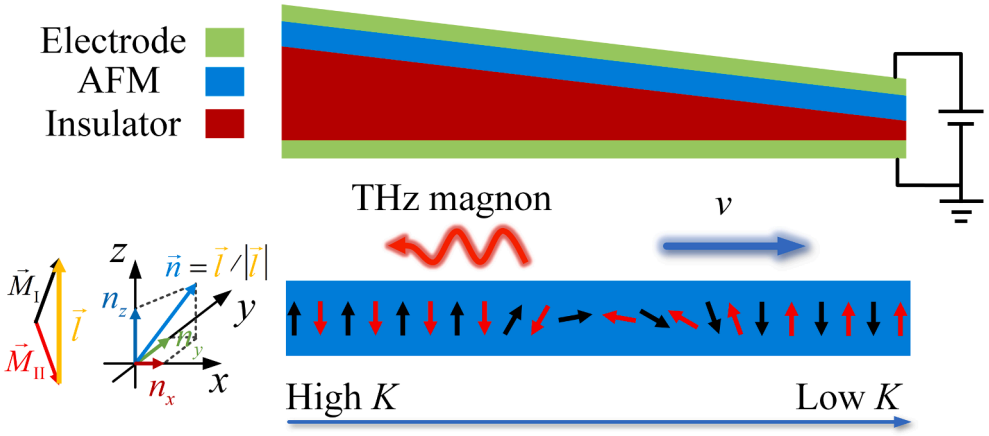

Fig. 1. Schematic of the calculation model: excitation of THz magnon from a moving AFM DW triggered by voltage-controlled magnetic anisotropy gradient. The Néel vector ($\vec{n}$) and its x-, y-, and z- components (n_x, n_y, and n_z) were defined near the figure of the 1-D AFM chain.

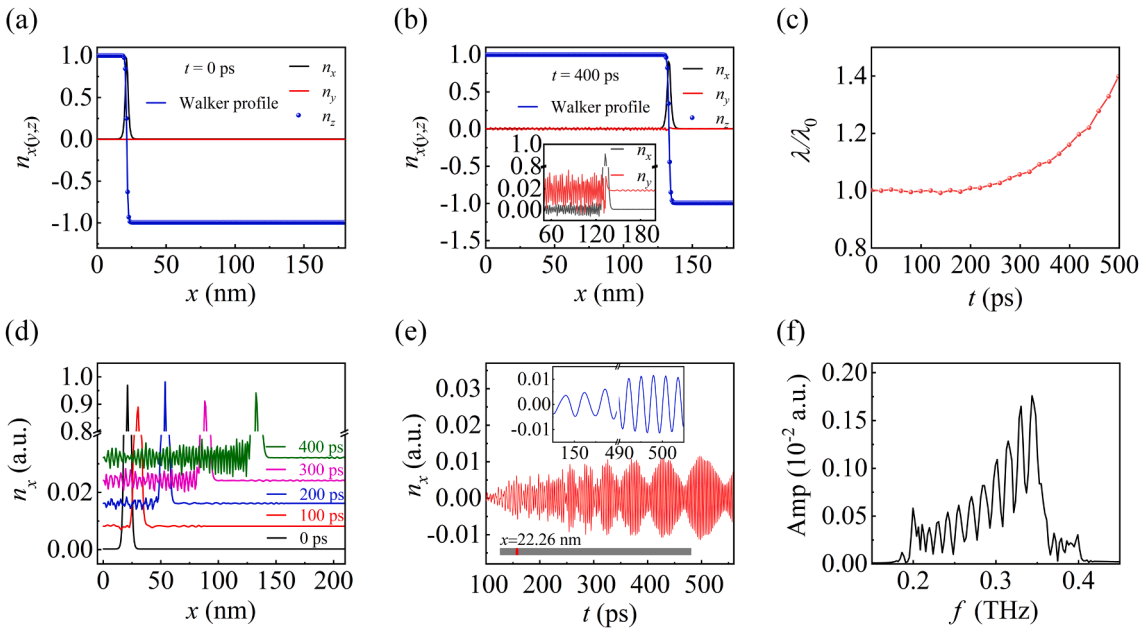

Fig. 2. Configurations for the *x*-, *y*-, and *z*-component of the Néel vector (n_x, n_y, and n_z) at (a) time $t = 0$ ps and (b) $t = 400$ ps, respectively. The DW profiles were fitted by the Walker function: $n_z = \cos[2\arctan(x - X)/\lambda]$(solid blue lines). Inset: enlarged profiles of n_x and n_y near the DW. (c) Relative variation of DW width λ/λ_0 with t at the anisotropy gradient $s = -1400$ GJ/m^4. Here λ_0 and λ indicate the DW width at 0 ps and that at t, respectively. (d) n_x as a function of x at various t for $s = -1400$ GJ/m^4. (e) n_x as a function of t at $x = 22.26$ nm, which is near the left end of the AFM chain. Inset: Oscillation of n_x near 150 ps and 500 ps. (f) Spectra of n_x at $x = 22.26$ nm from 100 ps to 550 ps.

a higher characteristic frequency due to the inertia of an AFM DW [49,50]. From a microscopic point of view, a wider DW results in a smoother variation of spin orientation across the DW region, which depresses the canting of the neighboring spins and strengthens the AFM exchange field, giving rise to the spin oscillation at a higher frequency.

We further investigated the DW velocity and magnon excitation at different s (Fig. 3). When $s = -200$ GJ/m^4, the DW accelerated in the initial 250 ps and subsequently reached a steady velocity of around 56 m/s. At a larger s, the DW velocity kept increasing. Fig. 3(b) displayed the spatial n_x for different s at $t = 400$ ps. The magnon can be excited when $s = -400$ GJ/m^4 or higher, and the magnon amplitude increased with the absolute value of s. Fig. 3(c) depicted the evolution of the average power in a period T (50 ps) calculated by $P_{avr} = -\frac{\mu_0 M_S d^3}{T}\sum_i \int_0^T \vec{S}^{(i)} \cdot \frac{d\vec{H}_{eff}^{(i)}}{dt} dt$ [51]. Here the summation covers all the spins on the left of the DW. The temporal P_{avr} indicates that the DW started to excite magnons at around 100 ps when s was -400 GJ/m^4 or higher [Fig. 3(c)]. To elucidate the dependence of magnon frequency on

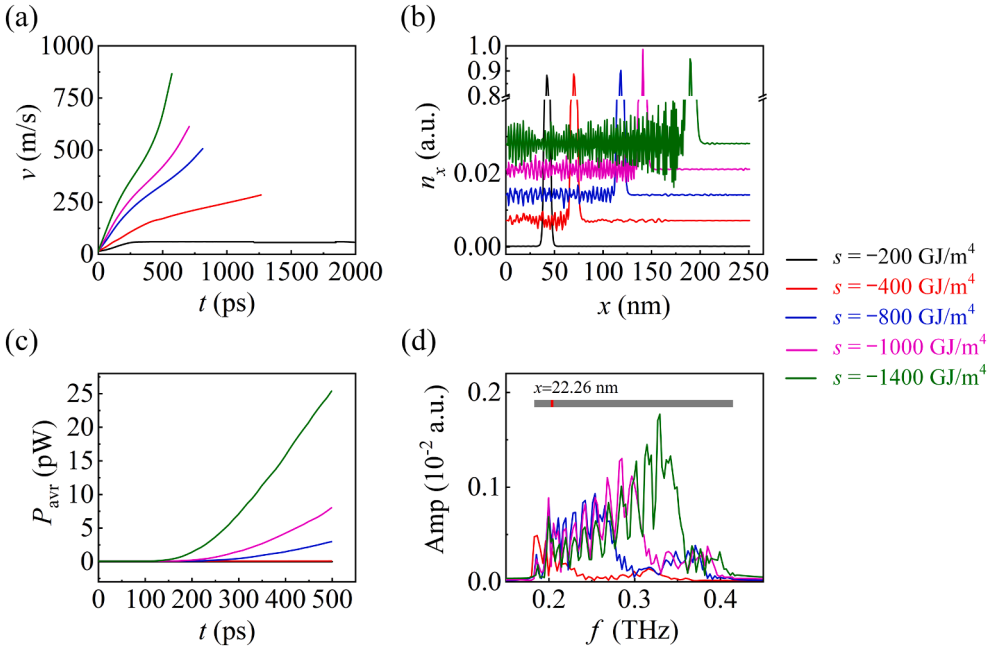

Fig. 3. DW motion and magnon excitation at different anisotropy gradient s. (a) Temporal DW velocity v vs time t. (b) Snapshots of the x-component of Néel vector (n_x) at $t = 400$ ps. (c) Average magnon power P_{avr} as a function of time t. Here the P_{avr} was calculated based on the n_x oscillation on the left of the DW. (d) Evolution of spectra for n_x oscillation from 100 ps to 500 ps at $x = 22.26$ nm as indicated in the inset.

s, we further analyzed the frequency for the n_x oscillation from 100 ps to 500 ps at $x = 22.26$ nm based on the 1D FFT (0.1-ps sampling interval). When $s = -400$ GJ/m^4, the magnon frequency was near 0.2 THz. More high-frequency modes between 0.2 and 0.4 THz were excited with the enhancement of s from -400 GJ/m^4 to -1400 GJ/m^4.

The complicated time and space dependence of n_x in Figs. 2 and 3 originates from the variation of frequency and the presence of the anisotropy gradient. In the Supplementary Materials (S2), we verified that the magnon profile at a sloped anisotropy is very different from that of a simple harmonic spin oscillation for a constant anisotropy.

The magnon excitation from a moving AFM DW depends on the properties of both the AFM chain and DW. We collected the magnon spectra at different positions of an AFM chain with an anisotropy gradient and presented the upper and lower frequency limit at these positions [the black and red dotted lines in Fig. 4(c) and (d)]. The magnon was excited by an alternating field as sinc function of time [52]: $\vec{h}(t) = h_{\max}\mathrm{sinc}\left[2\pi f_c(t-t_0)\right]\vec{e}_x$ in the region between $x = 124.74$ nm and $x = 126.42$ nm. Here $h_{\max}$ is the maximum exciting field strength (6 mT), and f_c is the cutoff frequency (5 THz), and $t_0 = 0.25$ ns. The n_x oscillation near 0.2 THz corresponds to a uniform precession at the gap frequency (f_g), whereas that around 0.4 THz denotes a spin wave with a wavelength comparable to the mesh size, which corresponds to the upper limit of the frequency (f_u). The variation of K_z in the AFM chain modified both f_g and f_u. Also, we studied the spin precession within the DW. We considered the oscillation of the azimuthal angle Φ of the Néel vector near the left end of the DW (4.2 nm from the DW center), which is the magnon source. We simulated the frequency of Φ (f_Φ) as a function of DW velocity [the blue and purple dotted lines in Fig. 4(c) and (d)]. At $s = -1400$ GJ/m^4, Φ weakly oscillated at a low f_Φ when $t < 80$ ps. Subsequently, both the frequency and amplitude were significantly enhanced, and f_Φ became greater than f_g when $t > 100$ ps [Fig. 4(d)], which matches the starting point of the magnon excitation in the temporal P_{avr} [Fig. 3(c)]. At $s = -200$ GJ/m^4, f_Φ approached a stable value that was well below f_{low} when the DW velocity also reached a stable value of around 56 m/s as labeled by v_s in Fig. 4(c). Therefore, no magnon can be excited.

The results in Fig. 4 indicated that the magnon excitation originates from resonant DW precession. Unlike the coupling between translation and precession of an FM DW, the translation of an AFM DW is generally thought to be decoupled with DW precession unless the acceleration is nonzero [35,36]. Nevertheless, in this work, we found obvious DW precession when the DW acceleration was negligible at $s = -200$ GJ/m^4 [inset of Fig. 4(a)]. This hints extra contribution of s to the DW precession.

To unravel the DW precession under a magnetic anisotropy gradient, we derived the dynamic equations for X and Φ by using the collective coordinate method. The Lagrangian of a moving DW is:

$$L = E_k - E_p \tag{3}$$

Here E_k and E_p are the kinetic and potential energy of the AFM system, respectively, and they were expressed as [53]:

$$E_k = S_\perp \int \frac{1}{2a\gamma^2}\dot{\vec{n}}^2 dx; \tag{4}$$

$$E_p = S_\perp \int \left[\frac{A}{2}\vec{n}'^2 - \frac{K_z}{2}n_z^2 - \frac{K_x}{2}n_x^2\right] dx \tag{5}$$

In Eqs. (4) and (5), a and A are the homogenous and inhomogeneous exchange constant, respectively.$S_\perp$ is the cross-section area of the AFM chain.

$\vec{n}$ was expressed in a spherical coordinate system as$\vec{n} =$

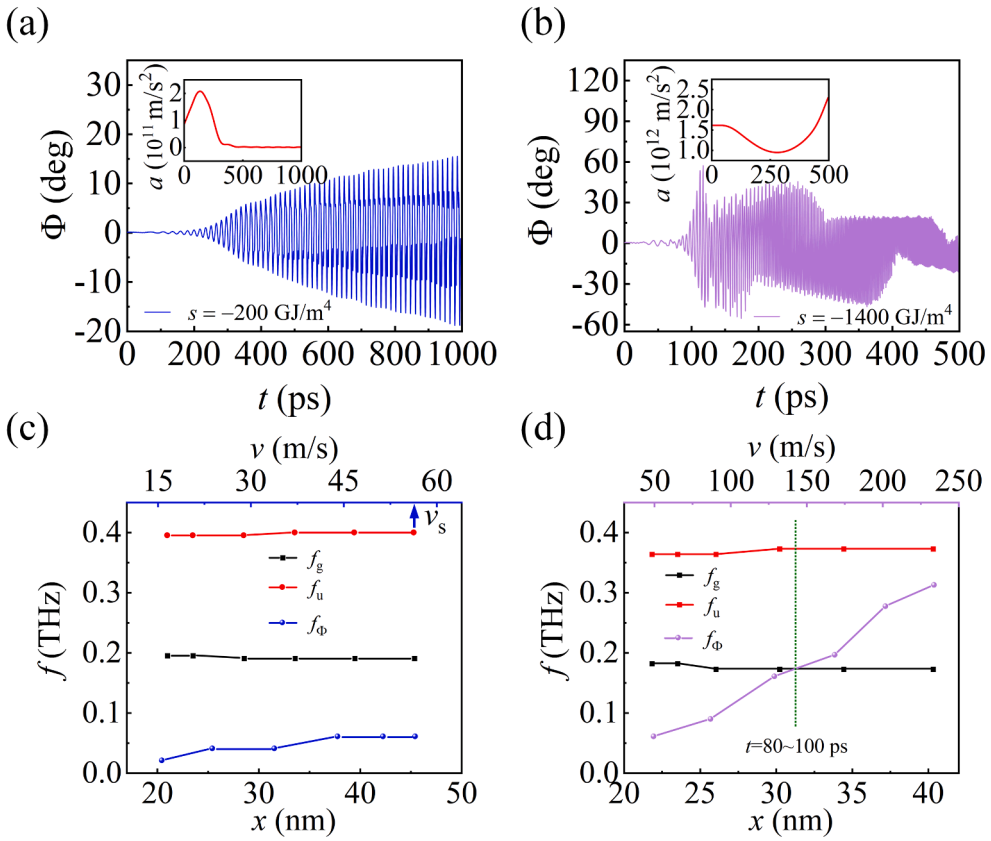

Fig. 4. Oscillation of azimuthal angle (Φ) of the Néel vector x-component (n_x) near the left edge of the DW (4.2 nm from the DW central) at (a) the anisotropy gradient $s = -200$ (the blue line) and (b) -1400 GJ/m^4 (the purple line). The inset indicates DW acceleration a. Frequency gap (f_g) and upper limits of the frequencies (f_u) at different positions and the frequencies of Φ (f_Φ) as a function of DW velocity v for (c) $s = -200$ and (d) -1400 GJ/m^4.

$(\sin\theta\cos\Phi,\ \sin\theta\sin\Phi,\ \cos\theta)$, where θ and Φ are the polar angle and azimuthal angle, respectively. Without the consideration of complicated spatial variation of Φ in the DW, the Lagrangian can be expressed by θ and Φ as:

$$L = S_{\perp}\int_{-\infty}^{+\infty}[\frac{\rho}{2}[\dot{\theta}^2+\sin^2\theta\dot{\Phi}^2]-\frac{A}{2}\theta'^2-\frac{K_z}{2}\sin^2\theta+\frac{K_x}{2}\sin^2\theta\cos^2\Phi]dx \tag{6}$$

Here $\rho=\frac{1}{a\gamma^2}=\frac{A}{c_{\max}^2}$ with $c_{\max}$ the maximum group velocity.

We exploited the Walker profile of an AFM DW: $\theta = 2\arctan[\exp(\frac{x-X(t)}{\lambda})]$ and$\Phi = \Phi(t)$. Here the DW width was expressed as $\lambda=\sqrt{A}\beta f^{-1/2}$ with $f = K_z - K_x\cos^2\Phi-\frac{\dot{\Phi}^2}{a\gamma^2}=K_0+sX-K_x\cos^2\Phi-\frac{\dot{\Phi}^2}{a\gamma^2}$ and$\beta=\sqrt{1-\frac{\dot{X}^2}{c_{\max}^2}}$, representing the softening effect from DW precession and Lorentz contraction, respectively. Inserting the Walker solution into the Lagrangian [Eq. (6)] and using the integral $\int_{-\infty}^{+\infty}\mathrm{sech}^2(\varepsilon)d\varepsilon=2$ and$\int_{-\infty}^{+\infty}\varepsilon^2\mathrm{sech}^2(\varepsilon)d\varepsilon=1.644$, we deduced the Lagrangian as:

$$\begin{aligned}L &= L_0+L_1\\ &= S_{\perp}\sqrt{A(K_z-K_x\cos^2(\Phi)-\rho\dot{\Phi}^2)}\sqrt{1-\frac{\dot{X}^2}{c^2}}\left[-2+0.822\left(\frac{\dot{\lambda}^2}{c^2-\dot{X}^2}\right)\right]\end{aligned} \tag{7}$$

where

$$\begin{aligned}L_0 &= -2S_{\perp}\sqrt{A(K_z-K_x\cos^2(\Phi)-\rho\dot{\Phi}^2)}\sqrt{1-\frac{\dot{X}^2}{c^2}}\\ &= -2S_{\perp}\beta\sqrt{Af}\end{aligned} \tag{8}$$

$$\begin{aligned}L_1 &= 0.822S_{\perp}\sqrt{A(K_z-K_x\cos^2(\Phi)-\rho\dot{\Phi}^2)}\sqrt{1-\frac{\dot{X}^2}{c^2}}\left(\frac{\dot{\lambda}^2}{c^2-\dot{X}^2}\right)\\ &= 0.822S_{\perp}\beta\sqrt{Af}\left(\frac{\dot{\lambda}^2}{c^2-\dot{X}^2}\right)\end{aligned} \tag{9}$$

We estimated $\frac{\dot{\lambda}^2}{c^2-\dot{X}^2}$ based on the numerical calculation results and found it is$<10^{-4}$ at the largest s (-1400 GJ/m^4). Therefore, we only considered L_0 in the following derivation. Eq. (8) was then put into the Euler-Lagrange Equation without considering the dissipation:

$$\frac{d}{dt}\left(\frac{\partial L_0}{\partial\dot{X}}\right)-\frac{\partial L_0}{\partial X}=0 \tag{10}$$

After a series of differential calculations, we finally derived the dynamics equation of X:

$$[K_x\sin(2\Phi)-2\rho\ddot{\Phi}]\frac{\dot{\Phi}\dot{X}}{c_{\max}^2}+2\left[K_0+sX-K_x\cos^2\Phi-\rho\dot{\Phi}^2\right]\frac{\ddot{X}}{c_{\max}^2-\dot{X}^2}+s=0 \tag{11}$$

Analytically solving Eq. (11) is rather unlikely. However, its physical meaning is still quite clear. When $s=0$, Eq. (11) leads to $\dot{X}\dot{\Phi}=0$ at a zero$\ddot{X}$. This indicates that DW precession is inhibited for uniform DW motion, which is consistent with the theoretical prediction by G. Tatara [35]. However, at a nonzero s, $\dot{X}\dot{\Phi}$ must be nonzero in the absence of DW acceleration. This confirms the coexistence of DW translation and precession and satisfies our numerical results [Fig. 4(a)].

Without $\ddot{X}$(a constant $\dot{X}$), Eq. (11) was further converted into.

$$2\rho\ddot{\Phi}-K_x\sin(2\Phi)=\frac{sc_{\max}^2}{\dot{X}\dot{\Phi}} \tag{12}$$

Here, $\frac{sc_{\max}^2}{\dot{X}\dot{\Phi}}$ represents the force exerted by the magnetic anisotropy gradient, which is modulated by$\dot{\Phi}$. This equation is analogous to the dynamics equation for a pendulum with a varying amplitude under a self-modified force. At a larger s, DW acceleration can't be neglected. In addition to s, $\ddot{X}$ also contributes to DW precession [the second term in Eq. (11)].

Finally, we estimated the electric-field strength for the magnon excitation. We assumed that K_z changes linearly with electric field strength (E) as:$\Delta K_z = \eta E$. Here $\eta=-\frac{3\lambda_s Y}{2(1-\nu^2)}(\nu d_{32}+d_{31})$ [54,55]. λ_s, Y, and ν are the saturation magnetostriction constant, Young's Modulus, and Poisson's ratio of NiO, respectively ($\lambda_s = 140$ ppm, $Y = 190.5$ GPa, $\nu = 0.399$) [56–58]. d_{31} and d_{32} are piezoelectric constants of a single-crystal PMN-PT ($d_{31} = -1750$ pC/N, $d_{32} = 900$ pC/N) [54]. Based on these parameters, $\eta = 6.62\times10^{-2}$ JV^{-1}m^{-2}. For $s = -400 \sim -1400$ GJ/m^4 with 1 nm thick NiO, and ΔK_z is between 1.01×10^5 and 3.53×10^5 J/m^3, and the maximum E is $1.52 \sim 5.33$ mV/nm, which corresponds to a 1-V voltage for a piezoelectric insulating layer with a thickness of about 1 μm. This shows that the THz magnon can be excited under a moderate voltage, verifying that the proposed method is expected to exhibit an ultralow power, avoiding current-induced or laser-induced heating.

4. Summary

In summary, we predict the excitation of THz magnons from a moving AFM DW under a magnetic anisotropy gradient. The magnon emission originates from the DW precession under an anisotropy gradient, and this DW precession is possible in the absence of DW acceleration, which is distinct from the previous reports. When the frequency of the DW precession is greater than the frequency gap of the magnon propagating in the AFM chain, THz magnons are excited from the DW. The magnetic anisotropy gradient can be generated under a moderate electric field, overcoming the thermal side effects from lasers or current. Our work paves the way to develop a voltage-controlled THz magnon device for future high-speed information processing.

CRediT authorship contribution statement

Xu Ge: Conceptualization, Methodology, Validation, Investigation, Writing – original draft. **Yangyi Chen:** Methodology, Validation, Software, Investigation. **Zaidong Li:** Methodology, Software. **Peng Yan:** Conceptualization, Methodology, Supervision, Funding acquisition. **Hong-Guang Piao:** Investigation. **Wei Luo:** Investigation, Funding acquisition. **Shiheng Liang:** Writing – review & editing. **Xiaofei Yang:** Conceptualization, Resources. **Long You:** Conceptualization, Resources. **Yue Zhang:** Conceptualization, Resources, Writing – review & editing, Supervision, Project administration, Funding acquisition.

Declaration of Competing Interest

The authors declare that they have no known competing financial interests or personal relationships that could have appeared to influence the work reported in this paper.

Data availability

Data will be made available on request.

Acknowledgment

The authors acknowledge financial support from the National Key Research and Development Program of China (Grant No. 2022YFE0103300), and the National Natural Science Foundation of China (Nos. 51971098, 11874169, 12074057, and U2141236), and the Program of State Key Laboratory of Quantum Optics and Quantum Optics Devices, Shanxi University, China (Grant No. KF202203).

Appendix A. Supplementary material

Supplementary data to this article can be found online at https://doi.org/10.1016/j.jmmm.2022.169858.

References

[1] V. Baltz, A. Manchon, M. Tsoi, T. Moriyama, T. Ono, Y. Tserkovnyak, Rev. Mod. Phys. 90 (2018), 015005.
[2] B.F. Ferguson, X.-C. Zhang, Nat. Mater. 1 (2002) 26.
[3] J. Walowski, M. Münzenberg, J. Appl. Phys. 120 (2016), 140901.
[4] Z. Feng, H. Qiu, D. Wang, C. Zhang, S. Sun, B. Jin, W. Tan, J. Appl. Phys. 129 (2021), 010901.
[5] A. Kirilyuk, A.V. Kimel, T. Rasing, Rev. Mod. Phys. 82 (2010) 2731.
[6] T. Kampfrath, A. Sell, G. Klatt, A. Pashkin, S. Mährlein, T. Dekorsy, M. Wolf, M. Fiebig, A. Leitenstorfer, R. Huber, Nat. Photonics 5 (2011) 31.
[7] T. Seifert, S. Jaiswal, U. Martens, J. Hannegan, L. Braun, P. Maldonado, F. Freimuth, A. Kronenberg, J. Henrizi, I. Radu, E. Beaurepaire, Y. Mokrousov, P. M. Oppeneer, M. Jourdan, G. Jakob, D. Turchinovich, L.M. Hayden, M. Wolf, M. Münzenberg, M. Kläui, T. Kampfrath, Nat. Photonics 10 (2016) 483.
[8] Y. Wu, M. Elyasi, X. Qiu, M. Chen, Y. Liu, L. Ke, H. Yang, Adv. Mater. 29 (2017) 1603031.
[9] M. Chen, R. Mishra, Y. Wu, K. Lee, H. Yang, Adv. Opt. Mater. 6 (2018) 1800430.
[10] A.V. Kimel, B.A. Ivanov, R.V. Pisarev, P.A. Usachev, A. Kirilyuk, T. Rasing, Nat. Phys. 5 (2009) 727.
[11] T. Satoh, S.-J. Cho, R. Iida, T. Shimura, K. Kuroda, H. Ueda, Y. Ueda, B.A. Ivanov, F. Nori, M. Fiebig, Phys. Rev. Lett. 105 (2010), 077402.
[12] V. Lopez-Dominguez, H. Almasi, P.K. Amiri, Phys. Rev. Appl. 11 (2019), 024019.
[13] A. Barra, J. Domann, K.W. Kim, G. Carman, Phys. Rev. Appl. 9 (2018), 034017.
[14] N.B. Weber, H. Ohldag, H. Gomonaj, F.U. Hillebrecht, Phys. Rev. Lett. 91 (2003), 237205.
[15] J. Wu, D. Carlton, J.S. Park, Y. Meng, E. Arenholz, A. Doran, A.T. Young, A. Scholl, C. Hwang, H.W. Zhao, J. Bokor, Z.Q. Qiu, Nat. Phys. 7 (2011) 303.
[16] N. Papanicolaou, Phys. Rev. B 51 (1995) 15062.
[17] J. Barker, O.A. Tretiakov, Phys. Rev. Lett. 116 (2016), 147203.
[18] X.S. Wang, P. Yan, Y.H. Shen, G.E. Bauer, X.R. Wang, Phys. Rev. Lett. 109 (2012), 167209.
[19] M. Yan, C. Andreas, A. Kákay, F. García-Sánchez, R. Hertel, Appl. Phys. Lett. 99 (2011), 122505.
[20] X.P. Ma, J. Zheng, H.G. Piao, D.H. Kim, P. Fisher, Appl. Phys. Lett. 117 (2020), 062402.
[21] T. Shiino, S.H. Oh, P.M. Haney, S.W. Lee, G. Go, B.G. Park, K.J. Lee, Phys. Rev. Lett. 117 (2016), 087203.
[22] W. Yu, J. Lan, J. Xiao, Phys. Rev. B 98 (2018), 144422.
[23] E.G. Tveten, A. Qaiumzadeh, A. Brataas, Phys. Rev. Lett. 112 (2014), 147204.
[24] L. Sánchez-Tejerina, V. Puliafito, P. Khalili Amiri, M. Carpentieri, G. Finocchio, Phys. Rev. B 101 (2020), 014433.
[25] H.Y. Yuan, W. Wang, M.-H. Yung, X.R. Wang, Phys. Rev. B 97 (2018), 214434.
[26] O. Gomonay, T. Jungwirth, J. Sinova, Phys. Rev. Lett. 117 (2016), 017202.
[27] H. Yang, H.Y. Yuan, M. Yan, H.W. Zhang, P. Yan, Phys. Rev. B 100 (2019), 024407.
[28] D.L. Wen, Z.Y. Chen, W.H. Li, M.H. Qin, D.Y. Chen, Z. Fan, M. Zeng, X.B. Lu, X. S. Gao, J.-M. Liu, Phys. Rev. Res. 2 (2020), 013166.
[29] P. Shen, Y. Tserkovnyak, S.K. Kim, J. Appl. Phys. 127 (2020), 223905.
[30] R. Yanes, M.R. Rosa, L. Lopez-Diaz, Phys. Rev. B 102 (2020), 134424.
[31] I. Gray, T. Moriyama, N. Sivadas, G.M. Stiehl, J.T. Heron, R. Need, B.J. Kirby, D. H. Low, K.C. Nowack, D.G. Schlom, D.C. Ralph, T. Ono, G.D. Fuchs, Phys. Rev. X 9 (2019), 041016.
[32] L. Baldrati, O. Gomonay, A. Ross, M. Filianina, R. Lebrun, R. Ramos, C. Leveille, T. Forrest, F. Maccherozzi, E. Saitoh, J. Sinova, M. Kläui, Phys. Rev. Lett. 123 (2019), 177201.
[33] S.-H. Oh, S.K. Kim, D.-K. Lee, G. Go, K.-J. Kim, T. Ono, Y. Tserkovnyak, K.-J. Lee, Phys. Rev. B 96 (2017) 100407(R).
[34] L. Caretta, S.H. Oh, T. Fakhrul, D.K. Lee, B.H. Lee, S.K. Kim, C.A. Ross, K.J. Lee, G. S. Beach, Science 370 (2020) 1438.
[35] G. Tatara, C.A. Akosa, R.M. Otxoa de Zuazola, Phys. Rev. Res. 2 (2020), 043226.
[36] X. Ge, Y.Y. Chen, Y. Cao, C. Li, T.L. Li, Z.Q. Li, L. You, S.H. Liang, X.Y. Yang, Y. Zhang, J. Phys. D: Appl. Phys. 55 (2022), 295302.
[37] Y. Zhang, S. Luo, X. Yang, C. Yang, Sci. Rep. 7 (2017) 2047.
[38] K. Yamada, S. Murayama, Y. Nakatani, Appl. Phys. Lett. 108 (2016), 202405.
[39] L. Chen, M. Shen, Y. Peng, X. Liu, W. Luo, X. Yang, L. You, Y. Zhang, J. Phys. D: Appl. Phys. 52 (2019), 495001.
[40] W.H. Li, Z. Jin, D.L. Wen, X.M. Zhang, M.H. Qin, J.-M. Liu, Phys. Rev. B 101 (2020), 024414.
[41] C. Ma, X. Zhang, J. Xia, M. Ezawa, W. Jiang, T. Ono, S.N. Piramanayagam, A. Morisako, Y. Zhou, X. Liu, Nano Lett. 19 (2019) 353.
[42] T. Conzelmann, S. Selzer, U. Nowak, J. Appl. Phys. 127 (2020), 223908.
[43] A. Parthasarathy, E. Cogulu, A.D. Kent, S. Rakheja, Phys. Rev. B 103 (2021), 024450.
[44] T. Chatterji, G.J. McIntyre, P.-A. Lindgard, Phys. Rev. B 79 (2009), 172403.
[45] T. Archer, C.D. Pemmaraju, S. Sanvito, C. Franchini, J. He, A. Filippetti, P. Delugas, D. Puggioni, V. Fiorentini, R. Tiwari, P. Majumdar, Phys. Rev. B 84 (2011), 115114.
[46] D. Ködderitzsch, W. Hergert, W.M. Temmerman, Z. Szotek, A. Ernst, H. Winter, Phys. Rev. B 66 (2002), 064434.
[47] W.-B. Zhang, Y.-L. Hu, K.-L. Han, B.-Y. Tang, Phys. Rev. B 74 (2006), 054421.
[48] B. Zhang, Z. Wang, Y. Cao, P. Yan, X.R. Wang, Phys. Rev. B 97 (2018), 094421.
[49] E.G. Tveten, A. Qaiumzadeh, O.A. Tretiakov, A. Brataas, Phys. Rev. Lett. 110 (2013), 127208.
[50] R. Rama-Eiroa, P.E. Roy, J.M. González, K.Y. Guslienko, J. Wunderlich, R. M. Otxoa, J. Magn. Magn. Mater. 560 (2022), 169566.
[51] R. Wieser, E.Y. Vedmedenko, R. Wiesendanger, Phys. Rev. B 79 (2009), 144412.
[52] M. Beg, M. Albert, M.-A. Bisotti, D. Cortés-Ortuño, W. Wang, R. Carey, M. Vousden, O. Hovorka, C. Ciccarelli, C.S. Spencer, C.H. Marrows, H. Fangohr, Phys. Rev. B 95 (2017), 014433.
[53] S.K. Kim, Y. Tserkovnyak, O. Tchernyshyov, Phys. Rev. B 90 (2014), 104406.
[54] M. Liu, O. Obi, J. Lou, Y. Chen, Z. Cai, S. Stoute, M. Espanol, M. Lew, X. Situ, K. S. Ziemer, V.G. Harris, N.X. Sun, Adv. Funct. Mater. 19 (2009) 1826.
[55] Z. Guo, X.F. Yang, J. Deng, B. Yan, J. Zheng, J. Ding, J. Li, B. Zhu, S. Chen, J. Ou-Yang, Y. Zhang, J. Alloys Compd. 687 (2016) 204.
[56] T.G. Phillips, R.G. White, Phys. Rev. 153 (1967) 616.
[57] Z.M. Zhou, Y. Zhou, C.S. Yang, J.A. Chen, G.F. Ding, W. Ding, M.J. Wang, Y. M. Zhang, Meas. Sci. Technol. 15 (2004) 2389.
[58] O. Seo, A. Tayal, J. Kim, C. Song, Y. Chen, S. Hiroi, Y. Katsuya, T. Ina, O. Sakata, Y. Ikeya, S. Takano, A. Matsuda, M. Yoshimoto, Sci. Rep. 9 (2019) 4304.